CHAPTER VI

RAPID ADSORPTION OF ARSENIC FROM AQUEOUS SLOUTION USING NANO ZERO-VALENT IRON COATED ON DIATOMITE: MECHANISM, KINETICS, AND RESPONSE SURFACE METHODOLOGY

A nanosized zero-valent iron coated on diatomite (nZVI-D) was synthesized for removing of arsenic in synthetic wastewater due to nZVI-D has a large surface area and a high reactivity. Three independent variables namely initial pH, initial concentration, and adsorbent dosage were investigated to study of arsenic adsorption. The optimal condition of As^{5+} removal was initial pH solution of 5.89, adsorbent dosage of 0.882 g/L, initial As concentration of 325 µg/L which 96.96% of As^{5+} could be eliminated in 1 min. An As^{3+} can be removal completely in 1 min by using the amount of nZVI-D of 0.925 g/L, pH 2.6 and initial concentration of 1,175µg/L. The adsorption kinetics and adsorption isotherm of As^{5+} and As^{3+} were found to follow the pseudo-second-order kinetic model and Langmuir adsorption isotherm, respectively. It can be concluded that the removal process was controlled by mass transfer and adsorption process which has monolayer adsorption and chemisorptions.

The XANES and XPS results were shown the oxidation state of iron in structures was changed from Fe foil to Fe_2O_3. The data was confirmed that arsenate was adsorbed onto the nZVI-D_2. There are 4 methods for As^{5+} removal by using nZVI-D_2 including reaction process, ions attraction, solid-phase redox transformation and adsorptions. The As^{5+} was accumulated on nZVI-D_2 in the form of As^0, FeH_2AsO_4, FeOAsOOH and As-Al/Si while the removal of As^{3+} increased the oxidation process.

This paper is accepted to published in the journal Environmental engineering science

6.1 Introduction

Arsenic contamination in drinking water is a very serious problem of global. The natural processes for the environmental spreading of arsenic are weathering reactions such as biological activities and volcanic emissions as well as human activities like mining, petroleum refineries and ceramic manufacturing industries (Mahmood et al., 2012). Arsenic is commonly found in water in the form of inorganic species. The major of arsenate species are $H_2AsO_4^-$ and $HAsO_4^{2-}$ and arsenite species is H_3AsO_3 (Kanel, Grenèche, & Choi, 2006a). Various arsenic species depending on pH, redox potential are factors these affect arsenic speciation in water. Normally, As^{3+} is found in ground water than As^{5+}.

The exposes of arsenic via drinking water and food caused lung, liver, kidney and bladder cancer. The arsenic compounds have been classified as Group I carcinogens (Straif et al., 2009). Therefore, the contamination limit for arsenic in drinking water 10 µg/L was set by World Health Organization (WHO, 2012) Even through, there are legislate environmental to control the using of arsenic and its compounds, the arsenic compounds still widely used in agricultures, ore mine, electronics, pharmaceuticals, and the ceramic industry. Consequently, arsenic concentration of treated waters should lower than 10 µg/L. It is necessary to develop methods for arsenic removal from aqueous environment for achieves low cost, simple, and fast technology.

Recently, several methods are used to treatment arsenic contamination such as precipitation, electrochemical reduction, adsorption, ion exchange, and reverse osmosis (Manning, Hunt, Amrhein, & Yarmoff, 2002), which have limitaton on treatment as low concentration of metals and cost effective. Newly, nanoscale zero-valent iron (nZVI) has been utilized for treatment of arsenic contaminated in aqueous environment (Bhowmick et al., 2014; Gutierrez-Muñiz, García-Rosales, Ordoñez-Regil, Olguin, & Cabral-Prieto, 2013; Kanel, Grenèche, & Choi, 2006; Manning et al., 2002). Many reports indicated that nZVI can treat environmental contaminants such as inorganic pollutants and heavy metals (Arshadi, Soleymanzadeh, Salvacion, & Vahid, 2014; Yun, Cho, Jang, & Park, 2013; Zhuang et al., 2011; Zhu et al., 2013) because of its large active surface area and high adsorption capacity. nZVI acts as certain material for removal of heavy metals from aqueous solution. However, the

agglomeration of nZVI decreased the reactivity of the particle and also reduced mobility and transport of nZVI to the contaminated area (Arshadi et al., 2014; Bhowmick et al., 2014; Wang et al., 2014). Thus, the loading nZVI onto supporting material has the potential to become an effective agent for treating wastewater containing heavy metal.

Diatomite ($SiO_2 \cdot nH_2O$) is a natural amorphous siliceous mineral in the clay, which has soft and lightweight. The porous structure of diatomite mainly composed of silica and alumina. It is suitable to be supporting material due to its property of catalysis. According to diatomite is cheap and easily purchase. Hence, diatomite is suitable to be supported material. Previous research, nZVI on the support is known to eliminate heavy metals from aqueous solution (Bhowmick et al., 2014; Zhang, Li, Y. Li, J. Hu, & Zheng, 2011), but the application not widely use and uncertainly indicates mechanism of adsorption. Therefore, this research studies the preparation of adsorbent with new synthesize method. It can rapidly absorb arsenic, easy to handle and longtime store. nZVI-D_2 suit for arsenic absorption, in contrast the other synthesis method must be use immediately after the preparation.

6.2 Objectives

The main focuses are as follows: (i) study factor to remove arsenic ions with nano zero valent ion coated on diatomite (nZVI-D) by central composite design (CCD) with used as experiment designed: adsorbent dose, pH and initial concentration. (ii) examine the kinetic adsorption isotherms, adsorption isotherm models, and thermodynamic, and (iii) propose the mechanism of arsenic adsorption which confirmed by nZVI-D with X-ray Absorption Near Edge Spectroscopy (XANES) and an X-ray photoelectron spectroscope (XPS).

6.3 Experimental

6.3.1 Chemicals and materials

Diatomite powder with particle size of 150 micron was achieved from the North Thailand. Iron(III) sulphate ($FeSO_4 \cdot 7H_2O$), sodium borohydride ($NaBH_4$) and absolute ethanol were used in this study to achieve from Merck Company (Germany) and Ajax Finechem (Australia). All aqueous solutions were prepared with deionized

water which is purified with Millipore Milli-Q Plus water purification system. For batch adsorption experiments, 1 mg/L of As^{5+} stock solution was prepared by dissolving $Na_2HAsO_4 \cdot 7H_2O$ and $NaAsO_2$ was used for stock solutions of As^{3+}. Finally, the initial pH was adjusted using hydrogen chloride and sodium hydroxide.

6.3.2 Experimental design

A primary research (chapter V), adsorbent dose, initial concentration and pH are significant factors for As^{5+} adsorption using a Plackett–Burman Design (Pojananukij, Wantala, Neramittagapong, & Neramittagapong, 2014). In this purpose, the response surface methodology (RSM) based on a central composite design (CCD) was employed to study the effect of factors and their interactions which effect of As^{5+} and As^{3+} adsorption with nZVI-D. The significant variables were utilized adsorbent dose (X_1), pH (X_2) and initial concentration (X_3). Each variable was considered at five different levels in CCD: negative star, minimum, center, maximum and positive star points as -1.7, -1, 0, +1, and +1.7, respectively (Onal, & Rodrigues, 2014), shows in Table 6.1. All variables were taken at a central coded value, which was considered as zero. The full experimental plan with consider to their values in actual and coded form and a total of 20 experiments is shown in Table 6.2 of As^{5+} and Table 6.3 of As^{3+}.

Table 6.1 Experimental range and levels of independent process variables

Variables	Units	Symbol code	Levels				
			-1.7	**-1**	**0**	**+1**	**+1.7**
Adsorbent dose	g/L	X_1	0.075	0.250	0.500	0.750	0.925
pH	-	X_2	2.6	4.0	6.0	8.0	9.4
Initial concentration	µg/L	X_3	325	500	750	1,000	1,175

All the experiments were carried out in duplicate. The percentages As^{5+} removal was defined using the following equation:

$$Y = \frac{C_0 - C_t}{C_0} \times 100 \qquad (2.20)$$

where C_0 is the initial concentration of As^{5+} (mg/L) and C_t is the concentration of As^{5+} (mg/L) after adsorption at time. Y is the percentage As^{5+} removal.

Table 6.2 Central composite design designs with experimental value and predicted value of arsenate removal

Run order	Coded levels			As^{5+} remove (%)	
	X_1	X_2	X_3	Observed	Predicted
1	-1	-1	-1	26.691	27.473
2	1	-1	-1	71.636	71.627
3	-1	1	-1	25.771	26.774
4	1	1	-1	65.322	66.078
5	-1	-1	1	26.041	25.925
6	1	-1	1	66.769	66.407
7	-1	1	1	16.861	17.509
8	1	1	1	53.282	53.142
9	-1.7	0	0	9.862	8.808
10	1.7	0	0	76.459	76.626
11	0	-1.7	0	23.898	24.034
12	0	1.7	0	13.187	12.164
13	0	0	-1.7	81.681	80.501
14	0	0	1.7	67.856	68.189
15	0	0	0	61.478	63.095
16	0	0	0	63.961	63.095
17	0	0	0	62.513	63.095
18	0	0	0	62.329	63.095
19	0	0	0	64.753	63.095
20	0	0	0	61.964	63.095

Symbols: X_1 = Adsorbent dose, X_2 = pH, X_3 = Initial concentration

Table 6.3 Central composite design designs with experimental value and predicted value of arsenide removal

Run order	Coded levels			As^{3+} removal (%)		
	X_1	X_2	X_3	Replicate 1	Replicate 2	Predicted
1	-1	-1	-1	32.70	32.43	32.97
2	1	-1	-1	73.93	71.59	73.54
3	-1	1	-1	43.54	42.80	44.14
4	1	1	-1	52.17	51.62	50.89
5	-1	-1	1	36.13	34.09	35.94
6	1	-1	1	80.53	79.19	78.72
7	-1	1	1	25.96	24.37	24.21
8	1	1	1	33.59	33.91	33.17
9	-1.7	0	0	27.04	28.85	27.11
10	1.7	0	0	67.96	68.37	69.21
11	0	-1.7	0	62.62	59.97	60.68
12	0	1.7	0	30.69	30.57	31.46
13	0	0	-1.7	51.94	53.00	51.69
14	0	0	1.7	38.47	37.85	39.15
15	0	0	0	41.92	42.80	42.74
16	0	0	0	42.53	44.32	42.74
17	0	0	0	42.05	44.78	42.74
18	0	0	0	41.51	44.53	42.74
19	0	0	0	41.73	45.05	42.74
20	0	0	0	40.46	44.50	42.74

Symbols: X_1 = Adsorbent dose, X_2 = pH, X_3 = Initial concentration

6.3.3 Batch adsorption procedure of arsenate

Adsorption experiments were approved desired by experimental design. The adsorption experiments were carried out at 30°C. In each conical flask, 120 mL 325-1,250 µg/L As^{5+} solution and the adsorbent were added (0.075-0.925 g/L). With shaking at 160 rpm for a regular interval of time, the equilibrium was reached. The

initial pH of the solution was adjusted to 2.6-9.4 with 1 M HCl or NaOH. At regular intervals an aliquot of supernatant was sampled and filtered through 0.45-μm membrane filter (Millipore) for aqueous arsenic analysis.

The adsorption isotherms were studied in batch experiments. 120 mL of 11000, 1250, 1500, 1750, and 2000 μg/L As^{5+} solutions were added in a series of flasks, maintained at the optimum pH which adjusted to 6 with 1 M HCl or NaOH. Then nZVI-D_2 was added 0.09 g into each flask. The suspension was shaken for a period between 1 and 60 min with a rotary shaker at a speed of 150 rpm. The suspensions were filtered with syringe Filter Nylon 0.45-μm membrane (Lubitech, Thailand). The remaining concentration of arsenate was determined by Graphite furnace atomic absorption spectrometry (GFAAS), Perkin Elmer series Analyst 880, United States. The adsorption capacity (q_e (μg/g)) of nZVI-D_2 was calculated as follows:

$$q_e = \frac{(C_0 - C_t)}{M} V \tag{6.1}$$

where C_0 is initial concentration of arsenate solution (μg/L) and C_t is concentration of arsenate solution (μg/L) at time t; V is the volume of the solution (L); and M is mass of adsorbent (g).

6.4 Results and discussion of arsenate adsorption process

6.4.1 Optimization of arsenate adsorption process

The data in Table 6.2 was used to fit the polynomial model representing the response as function of initial pH, adsorbent dosage and initial concentration. According to the RSM results, polynomial regression modeling was operated between the responses of the corresponding coded values of the three different process variables. The analysis of variance (ANOVA) of regression parameters of the response surface methodology quadratic model for As^{5+} adsorption onto nZVI-D_2 are listed in Table 6.4. Furthermore, the ANOVA of the quadratic regression model indicated that the model was highly significant ($p < 0.0001$). The regression analysis of the experimental design reveals that the linear model terms of X_1, X_2 and X_3, the

quadratic model terms of X_1^2, X_2^2 and X_2^3 and the interaction model terms of X_1X_2, X_1X_3, X_2X_3 were highly significant ($P < 0.05$) shown in Table 6.4.

Table 6.4 ANOVA for the parameters of response surface quadratic model

Source	Sum of squares	df	Mean square	F-value	P-value
Model	20976.5	9	2330.7	775.01	0.000
Linear	11662.4	3	3887.5	1292.66	0.000
X_1	10965.1	1	10965.1	3646.11	0.000
X_2	335.9	1	335.9	111.71	0.000
X_3	361.4	1	361.4	120.16	0.000
Square	9217.5	3	3072.5	1021.67	0.000
X_1X_1	1060.3	1	1480.0	492.14	0.000
X_2X_2	7706.2	1	7216.2	2399.52	0.000
X_3X_3	451.1	1	451.1	149.99	0.000
Interaction	96.5	3	32.2	10.70	0.000
X_1X_2	23.5	1	23.5	7.82	0.009
X_1X_3	13.5	1	13.5	4.48	0.043
X_2X_3	59.5	1	59.5	19.80	0.000
Lack of fit	12.9	5	2.6	0.84	0.537
Pure error	77.3	25	3.1		
Residual	90.2	30	3		
Total	21066.7	39			

Symbols: X_1 = Adsorbent dose, X_2 = pH, X_3 = Initial concentration

$R^2 = 0.9957$, adjusted $R^2 = 0.9920$ and predicted $R^2 = 0.9944$

The *F*-value and p-value of lack of fit were 0.84 and 0.537 respectively, implying that the error of this model is insignificant. This model can be used to navigate the design space and the model was well fit. The equation model was employed to calculate which the predicated response is as follows:

$$Y = 63.095 + 19.946X_1 - 3.491X_2 - 3.621X_3 - 7.051X_1^2 - 15.569X_2^2 + 3.892X_2^3 - 1.212X_1X_2 - 0.917X_1X_3 - 1.929X_2X_3 \quad (6.2)$$

where Y is the response denoted as the predicted percentage As^{5+} adsorption. X_1, X_2 and X_3 are the corresponding coded variables of adsorbent dose, pH and initial concentration, respectively.

The experimental and predicted removal efficiency plot for As^{5+} is displayed in Fig. 6.1. It indicated that the predicted values of efficiency As^{5+} removal obtained from the model and the experimental data were well agreement. It provide evidence for the validity of the regression model showed a value of the determination coefficient (R^2) higher than 0.99. The closer the value of R^2 to unity, the empirical models fits the actual data (Onal, & Rodrigues, 2014; Tatineni, Doddapaneni, Potumarthi, & Mangamoori, 2007). Furthermore, a good statistical model, the adjusted determination coefficient (R^2_{adj}) closes to R^2. It only 0.1% of the total variations were not explained by the models.

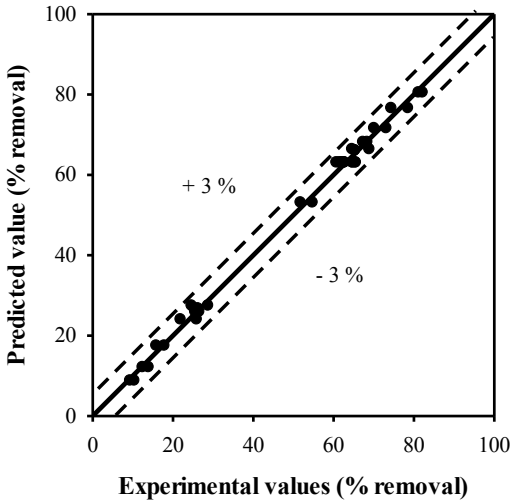

Figure 6.1 Correlation of experimental and predicted removal efficiency for As^{5+} with nZVI-D_2

It also indicated that a high degree of correlation between the observed and predicted values. It can be summarized the response surface model developed in this study for the prediction of As^{5+} removal (Eq. 6.3). To confirm the above equation that

can predict the adsorption of As^{5+}. Therefore, study the conditions of the calculated values match the value actual experiment. The results shown three replicated of experiment in conditions of 0.9 g/L, pH 6, 1,000 µg/g of initial concentration which given As^{5+} removal of 74.33 %, Standard deviation (SD) value equal 2.06, which is close to the predicted value (75.90%).

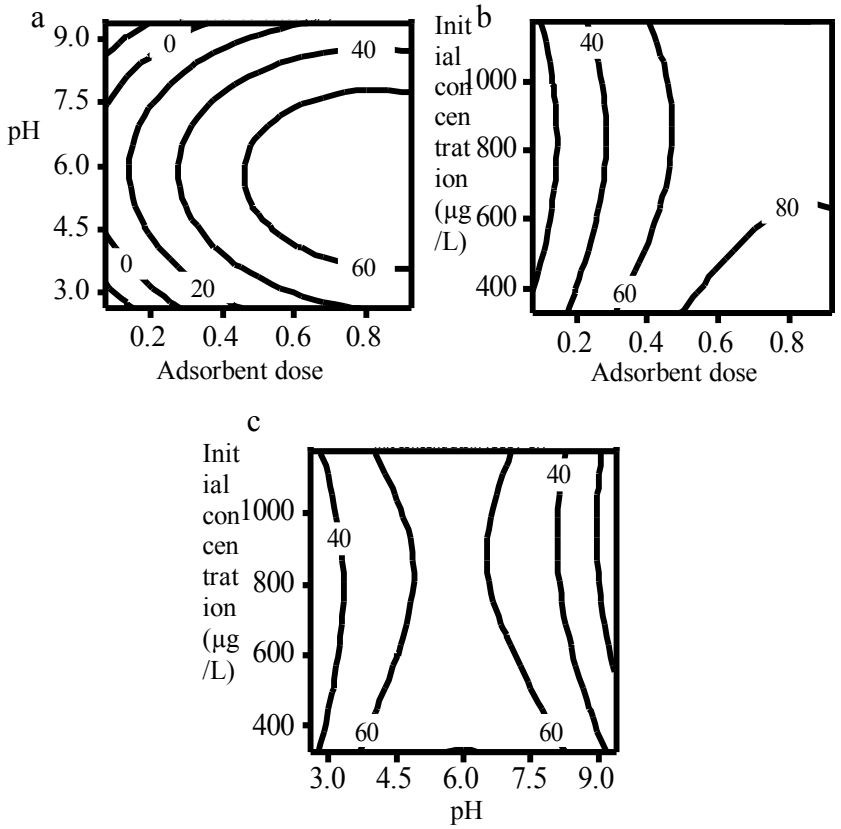

Figure 6.2 Contour plots for combined effect of (a) pH and adsorbent dose (b) initial arsenate concentration and adsorbent dose (c) initial concentration and pH on removal efficiency of arsenate at 1 min

The contour plots display the relationship between two variables and response value for formation response value and operating conditions. The contour data displayed the range of the high efficiency (71.90-96.96%) in the condition of the initial As^{5+} concentration as 325-600 µg/L , the pH value as 4.5-7.5 and the adsorbent dose as 0.5-0.9 g/L at reaction time of 1 min which shown in Fig 6.2. The experimental conditions for maximum As^{5+} removal (96.96%) were adsorbent dose

(X_1) of 0.8821 g/L, pH (X_2) of 5.89 and initial concentration (X_3) of 325 µg/L with reaction time at 1 min.

6.4.2 Effect of process variables

Contour plots were generated to consider the effect of three factors, such as adsorbent dose, pH and initial concentration on As^{5+} removal. The influences of the three different process variables on the response factors are shown in the Fig. 6.2.

6.4.2.1 Effect of adsorbent dose

The removal efficiency of As^{5+} rapidly increased with increase the adsorbent dose ranging from 0.075 to 0.882 g/L. Accordingly, the percentage As^{5+} adsorption increased with increasing the amount of adsorbent dose for the reason that the availability of active site on the adsorbent surface and functional enhance which making easier penetration of heavy metal to the adsorbent site (Cao, Wu, Jin, Yilihan, & Huang, 2014). On the other hand, the adsorbent dose ranging from 0.882 to 0.925 g/L, the removal efficiency of As^{5+} was significantly constant due to the reduction in concentration gradient. In addition it cause of overlapping or aggregation of adsorption sites resulting in a decrease in total adsorbent surface area (Senthil Kumar, 2014).

6.4.2.2 Effect of pH

The pH of the solution is one of the most important operating parameters which it affected the adsorption of metal ions. The pH values were studied in the range from 2.6 to 9.4. The percentage of adsorption increases slightly at the pH range of 2.6–6.0 and maximizes at pH 6.0 found that the highest removal efficiency of As^{5+} on the nZVI-D_2 as well as previous research (Bhowmick et al., 2014; Kanel et al., 2006). After pH 6.0, the adsorption of As^{5+} decreases significantly until pH 9.4. The pH value of solutions influences the protonation or deprotonation of the adsorbent surface as a result, a positive or negative surface can be form as the following (Elizalde-González, Mattusch, Wennrich, & Morgenstern, 2001):

$$\equiv \text{Fe-OH} + H^+ \leftrightarrow \equiv \text{Fe-OH}_2^+ \quad (6.3)$$

$$\equiv \text{Fe-OH} \leftrightarrow H^+ \equiv \text{FeO}^- \quad (6.4)$$

The predominate As^{5+} species in aqueous solution is $H_2AsO_4^-$ in the range of pH 2 to 6 which the adsorbent surface display positive ion at pH solution below pH_{pzc}. The adsorption was occurred by the reaction and electrostatics attraction force between ions of As^{5+} and the surface of nZVI-D_2 which leading to the formation of surface complexes. Contrary, the pH solution more than pH 6 as a results the As^{5+}adsorption decreases because of pH of solution more than pH_{pzc} which the nZVI-D_2 surface has negative ion. Therefore, the competition between $HAsO_4^{2-}/AsO_4^{3-}$ and OH^- ions for active sits on nZVI-D_2. More important, in this study the pH_{pzc} of nZVI has effect on the adsorption system more than pH_{pzc} of nZVI-D_2.

6.4.2.3 Effect of initial concentrations

The adsorption of As^{5+} with nZVI-D_2 was studied by different initial concentrations (325-1,250 µg/L). The removal efficiency of As^{5+} decreased when increases the initial concentrations ranging from 325-1,000 µg/L because of a constant adsorbent dose resulting the active sites and surface areas were limited (Liu, Wang, Yan, & Zhang, 2014). Another reason the formation of clusters of nZVI-D_2 particles which is result the surface area was decreased, when amount of solution ions increased and available sites limited for high concentrations. However, the initial concentration was 1,250 µg/L resulting efficiency As^{5+} removal increase. Wherewith the interaction between the solution of heavy metals and adsorbent which provided the necessary driving force to eliminate of the resistances to the mass transfer of As^{5+} between the aqueous and nZVI-D_2 (Arshadi et al., 2014) and increased the driving force of concentration (Örnek, Özacar, & Şengil, 2007).

6.4.2.4 Effect of interactive

In case of interactive effect between pH and adsorbent dosage the response was increased with increase in adsorbent dosage and decrease in pH. Fig 6.2, it was observed found that with increase adsorbent dosed there is significant increase in removal percentage. This may be due to the fact that higher adsorbent dosed increases the number of active sites and overall surface area of the adsorbent thus percentage removal increase when initial concentration was drop and adsorbent dosed was raised. Whereas, in case of pH and initial concentration there is significant increase in the removal percentage was observed. That is the pH range from 4.5 to 7.5

and initial concentration was decrease into percentage removal increase. Therefore, the pH increased resulted the arsenic at high concentration is precipitated.

6.4.4 Equilibrium adsorption models of arsenate

The Langmuir, Freundlich, and Dubinin-Radushkevich adsorption isotherm models were used to study the effect of initial As^{5+} concentration which could be shown by the following equation:

$$\frac{C_e}{q_e} = \frac{C_e}{q_m} + \frac{1}{q_m K_L} \tag{2.3}$$

$$\log q_e = \log k_F + \frac{1}{n} \log C_e \tag{2.5}$$

$$\ln q_e = \ln q_d - \beta \varepsilon^2 \tag{2.6}$$

The results were illustrated in Fig. 6.3a. The Langmuir model can assume monolayer adsorption onto homogeneous surface with a finite number of identical sites, while the Freundlich model is empirical in nature. The experimental of As^{5+} adsorption was fit well with the Langmuir models more than the Freundlich isotherm. Langmuir models demonstrate the formation of monolayer layer of As^{5+} at the surface of nZVI-D_2 and the maximum adsorption capacity (q_{max}) was 2,801.65 μg/g. In this present study, the values of R_L were in the range of 0-1 indicated absorption process can occur in nature, favorable for adsorption and nZVI-D can absorb As^{5+} well. As well as, the Freundlich model, the value of Freundlich constant (n) was 8.57 which greater than 1 implied that the adsorption was stronger interaction between nZVI-D_2 and As^{5+} solution and the adsorption process was heterogeneous and favorable adsorption (Fan et al., 2008) like with the Langmuir. Fig. 6.3b shows the results effect of time on adsorption of As^{5+} solution. These results also indicate that the removal process can be considered very fast because a significant amount of As^{5+} was adsorbed onto the sorbent within the first 10 min of adsorption which treated up to 90 %. In the range of 10 and 20 min, the percentages removal was slowly increases from 90-99 % whereas; at 30 min nZVI-D_2 can remove 100 % of As^{5+} solution. The results show that the initial adsorption rate is very rapid because of high available surface area and active site of adsorbent that enhance the interface and driving force. When

compared with the other research found that the equilibrium time was lower than the zero valent iron/active carbon (Dou, Li, Zhao, & Liang, 2010), zirconia nanoparticle (Zheng, Yu, Wu, & Paul Chen, 2012) and iron-modified carbon (Gutierrez-Muñiz et al., 2013).

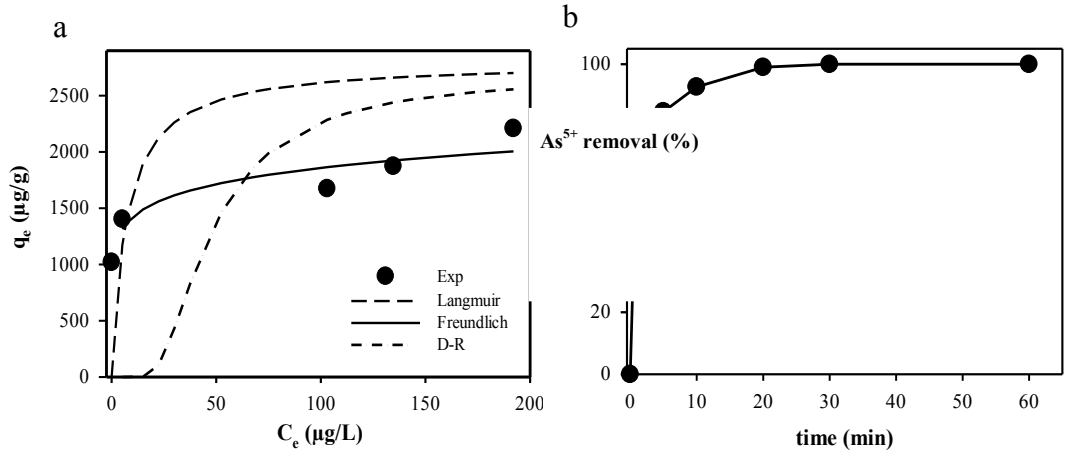

Figure 6.3 (a) adsorption isotherms of initial arsenate concentration: 1,000-2,000 µg/g, pH 6, adsorbent dose: 0.75g/L, equilibrium time: 60 min and temperature: 30 ºC (b) effect of time on adsorption value of arsenate at 1,000 µg/g

6.4.3 Kinetic adsorption isotherms of arsenate

In order to examine the diffusion mechanism involved during the adsorption process, the pseudo-first-order kinetic, pseudo-second order kinetic and intra-particle diffusion model model were tested, which could be show by the following equation:

$$\log\left(q_e - q_t\right) = \log q_e - \frac{k_1}{2.303}t \tag{2.9}$$

$$\frac{t}{q_t} = \frac{1}{k_2 q_e^2} + \frac{1}{q_e}t \tag{2.10}$$

$$q_t = k_i t^{1/2} \tag{2.12}$$

The adsorption kinetics isotherms were studied to ensure the mass transfer affected in the As^{5+} adsorption. It was explained by the pseudo-first order kinetic and the pseudo-second-order kinetic model. Table 6.5, it is clear that the R^2 value of the pseudo-first-order kinetic is lower than the pseudo-second-order kinetic which indicating that the pseudo-second-order kinetic were well fit with experimental kinetic data more than the pseudo-first-order kinetic. This suggests that As^{5+} adsorption were adsorbed onto the nZVI-D_2 by chemical interaction (Abdelwahab, & Amin, 2013). As the rate constant of pseudo second-order adsorption (k_2) was a complex coefficient and a basis of the mass transfer between adsorbate and adsorbent surface (Ma et al., 2014). In this study can be divided into two periods of k_2 (Fig. 6.4b). Period one, the k_2 increased with increasing initial concentrations in the low concentration (250-1,500 µg/L). In contrast the period another, k_2 decreased with increasing initial concentration in the high concentration (1,600-2,000 µg/L) since the less diffusion efficiency and a high competition of metal ions for fixed reaction sites, subsequently lower k_2 values were observed. It is obvious that the initial concentration of 1,500 µg/L is the best rate absorption.

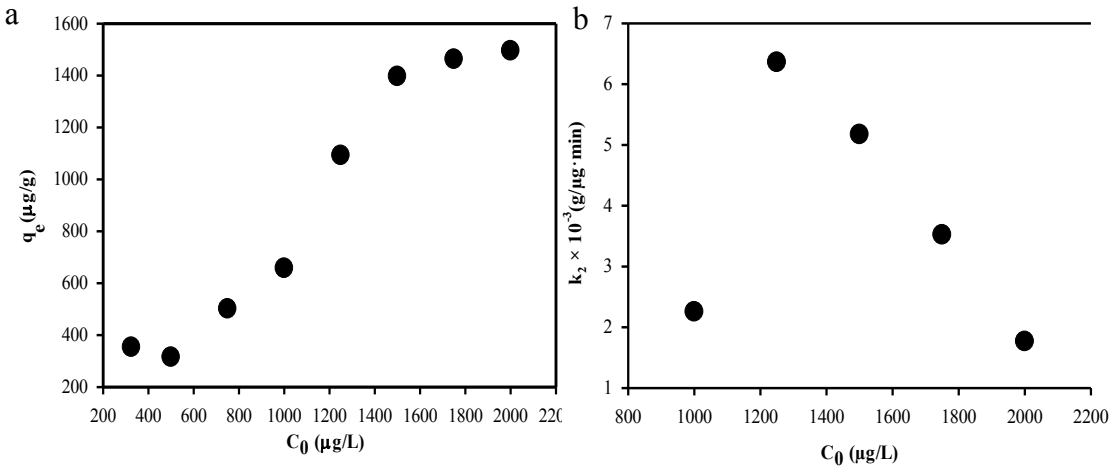

Figure 6.4 (a) adsorption capacity of the initial arsenate concentration (250–2,000 µg/g) at 1 min. (b) rate constant (k_2) of pseudo second-order adsorption (g/µg·min) at different initial arsenate concentrations (1,000-2,000 µg/g), pH 6, adsorbent dose: 0.75g/L, equilibrium time: 60 min and temperature: 30 ºC

Fig 6.4a shown the adsorption capacity of the initial As^{5+} concentration (250–2,000 µg/L) at 1 min resulting As^{5+} adsorption capacity efficiencies increased at 250–1,500 µg/L because adsorption capacity of nZVI-D_2 has not yet fully capable of absorbing. Nevertheless the adsorption capacity has almost constant at 1,600-2,000 µg/L indicating that the capacity of nZVI-D_2 (0.75g/L) reached a saturation point which cannot absorb any more. In addition, the rate constant of pseudo second-order adsorption (k_2) was decreased at initial As^{5+} concentration at 1,250-2,000 µg/L shown in Fig 6.4b.

Table 6.5 Kinetic parameters for the adsorption of arsenate onto nZVI-D_2 at the different concentrations

C_o (µg/L)	**1,000**	**1,250**	**1,500**	**1,750**	**2,000**
$q_{e,exp}$ (µg/g)	**1020.27**	**1403.16**	**1674.50**	**1874.19**	**2209.70**
pseudo-first-order					
$q_{e,cal}$ (µg/g)	443.19	322.01	349.17	452.98	696.82
$k_1 \times 10^{-2}$ (L/min)	3.61	2.44	4.94	5.70	4.28
R^2	0.895	0.557	0.811	0.841	0.807
pseudo-second-order					
$q_{e,cal}$ (µg/g)	1023.43	1360.14	1678.20	1884.41	2215.35
$k_2 \times 10^{-3}$ (g/µg·min)	2.25	6.35	5.17	3.52	1.76
R^2	0.997	0.999	0.999	0.999	0.999
intraparticle diffusion					
k_{i1}(mmol·µg·$min^{1/2}$)	26.49	156.22	195.70	314.75	506.90
k_{i2} (mmol·µg·$min^{1/2}$)	14.28	14.54	2.93	2.15	6.76

The pseudo-first-order and the pseudo-second-order kinetic unexplained the adsorption mechanism in the adsorption process of As^{5+} onto the nZVI-D_2, on the other hand the intra-particle diffusion model can explain. In the adsorption process, primary, the As^{5+} solution transferred form bulk solution into the external surface of nZVI-D (film diffusion). After that the solution molecules moved inside the adsorbent pores (intra-particle diffusion) and finally, As^{5+} solution was adsorbed onto the

interior surface of the pores and capillary spaces of nZVI-D_2 (adsorption). In fact, the intra-particle diffusion can be concluded that the adsorption process of As^{5+} characterized by either film diffusion or intra-particle diffusion. That was the line plot of q_t versus $t^{1/2}$ not passes through the origin, implying the intraparticle diffusion only was not the rate-limiting step but the film diffusion and intra-particle diffusion were the rate-limiting step (Chen et al., 2014; Ma et al., 2014). In sum up, the intra-particle diffusion plot can separate two linear. The first linear, the mass of As^{5+} solutions transferred across the bulk solution into the nZVI-D_2 surface (film diffusion). The second linear, the As^{5+} solutions were diffused into the nZVI-D_2 surface pores (intra-particle diffusion) (Bera, Kumar, Ojha, & Mandal, 2013).

6.4.5 Mechanism of arsenate adsorption on nZVI-D

The characteristics of Fe species after reaction were defined by the XANES. The XANES spectra found Fe^0, FeO, Fe_3O_4 and Fe_2O_3 were shown energy at 7111.69 eV, 7122.5 eV, 7122.5 eV and 7127.29 eV, respectively which displayed in Fig. 6.5. The XANES spectra of nZVI-D before adsorption was mainly detected of Fe^0 comparing with others iron references. While the XANES spectra of nZVI-D after adsorption arsenate was revealed three main peak such as FeO, Fe_3O_4 and Fe_2O_3 and was disappear of Fe^0in the reaction time at 20 min. That is the Fe^0 was oxidized on nZVI-D_2 surface. The ratio of iron oxidation state was presented in Table 6.6. The results proved that the oxidation state of iron in structures was changed by following $Fe^0 \rightarrow FeO \rightarrow Fe_3O_4 \rightarrow Fe_2O_3$, respectively.

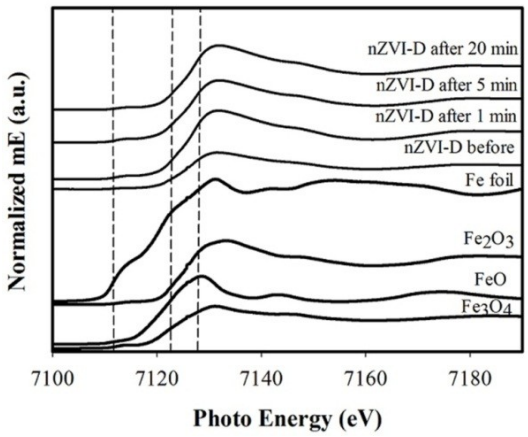

Figure 6.5 XANES spectrum of nZVI-D_2 with before and after adsorbed arsenate at 1-20 min. E_0 of Fe foil = 7111.69 eV, FeO = 7122.5 eV, Fe_3O_4 = 7122.5 eV, Fe_2O_3 = 7127.29 eV

The XPS analysis results were indicated that elements in the nZVI-D_2 were at Fe 2p 711.4 eV, O 1s 531.4 eV, C 1s 284.4 eV, Si 2p 102.4 eV and Al 2p 74.4 eV as shown in Fig 6.6a. The nZVI-D_2 (5 g/L) was added to 100 mg/L As^{5+} solution and reaction time 24 h. Subsequently, As^{5+} is adsorbed on the surface of nZVI-D_2, the iron oxide sites in the nZVI-D structure may potentially reduce As^{5+} to As^{3+} (Tu, You, Chang, & Wang, 2013) shown in Fig 6.6b. This is the XPS spectrum of As^{3+} had an absorption edge at 44.9 eV while that of $As^{5+}$was at 45.8 eV. However, the research of Weile Yan (Yan, Ramos, Koel, & Zhang, 2012) found that As^0 adsorb in the adsorbent. Moreover, the XPS analysis found Si-O, Si-OH, Si-O-M for Si 2p and Al metal for Al 2p which was created after adsorption display in Fig 6.6 (c-d). In is interesting note that, the peaks ratio of the oxygen at 531.5 and 532.3 eV increased after As^{5+} adsorption, suggesting that hydroxyl bonded to metal groups (M-OH) and metal oxide groups (M-O) construct on the surface of nZVI-D_2.

Table 6.6 Mass fraction of Fe species in nZVI-D_2 structures.

Adsorbent	Fe foil	FeO	Fe_2O_3	Fe_3O_4
nZVI-D before adsorption	0.2325	0.1484	0.4362	0.1829
nZVI-D after adsorption at 1min	0.0004	0.0002	0.8384	0.1610
nZVI-D after adsorption at 5min	0.0001	-	0.6922	0.3077
nZVI-D after adsorption at 20 min	-	0.0001	0.7455	0.2544

In this study considered the initial pH solution at pH 6 which the predominate specie of As^{5+} was mainly $H_2AsO_4^-$ in solution. Based on results of XANES and XPS can be suggested to the reaction of three section (4 pathway) of As^{5+}-nZVI-D_2 adsorption. The first section of reaction, the Fe^0 was oxide electron with water and oxygen, which a natural corrosion reaction is forms iron oxides and can act as an electron donor causing reduction of dissolved ions, as displayed by Eq. 6.6-6.8 (Bhowmick et al., 2014; X. Zhang, Lin, Chen, Megharaj, & Naidu, 2011). Then, the As^{5+} was reduced to As^0 by electrons produced from Fe^0. While As^{5+} can reduced to As^{3+} but possess was kinetically slow. Next, the As^0 diffused to near the oxide/Fe^0 interface explained by Eq. 6.9 and Fig 6.7 (Reduction path 1).

$$Fe^0 + 2H_2O \rightarrow Fe^{2+} + H_2 + 2OH^- \quad (6.5)$$

$$2Fe^0 + 2H_2O + O_2 \rightarrow Fe^{2+} + 4OH^- \quad (6.6)$$

$$2Fe^{2+} + H_2O + 0.5O_2 \rightarrow 2Fe^{3+} + 2OH^- \quad (6.7)$$

$$Fe^0 + H_2AsO_4^- + H_2O/O_2 \rightarrow Fe^{2+}/Fe^{3+} + As^0 + H_2 \quad (6.8)$$

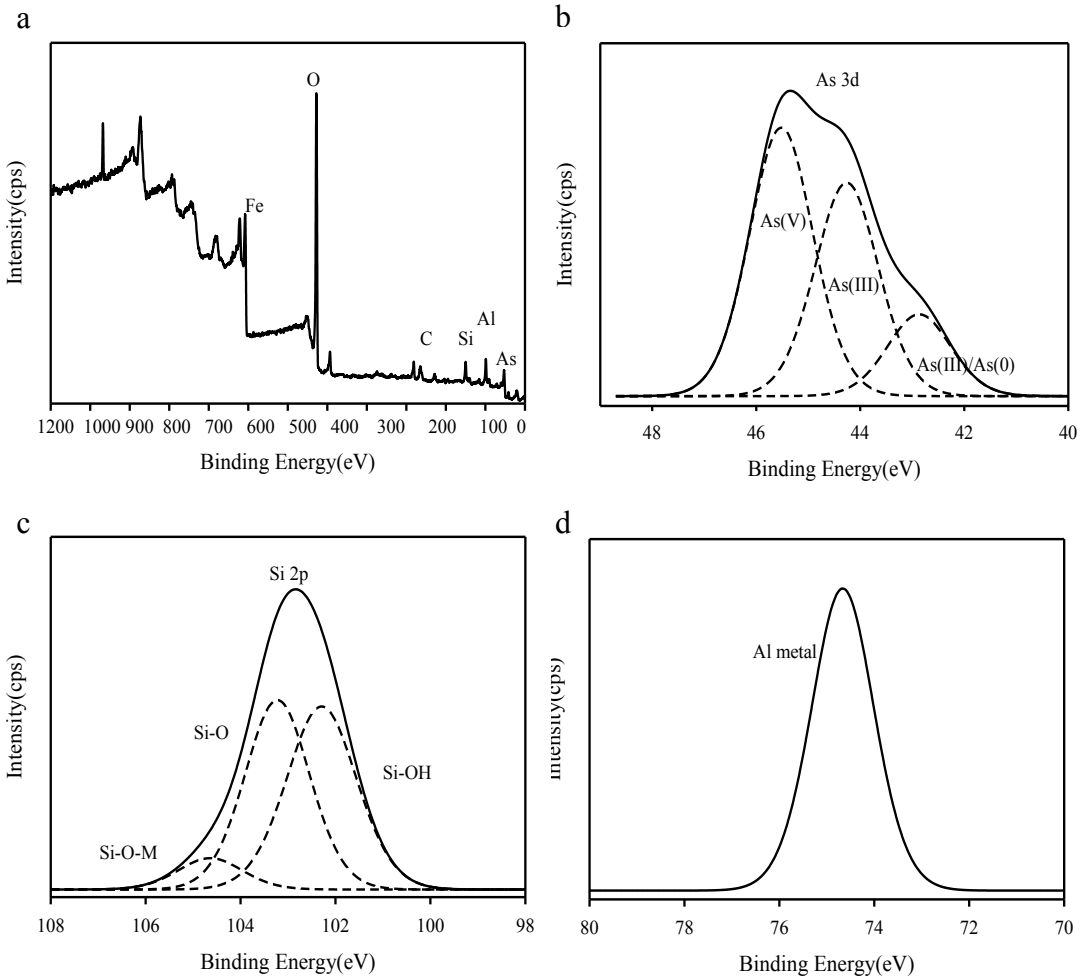

Figure 6.6 XPS spectra of (a) full survey of nZVI-D (b) As 3d (c) Si 2p (d) Al 2p in after adsorption 100 mg/L of arsenate solution with nZVI-D_2 with, 24 hr

The second section, the ions were attracted together between $H_2AsO_4^-$ and ferrous/ferric oxides surface sites then iron arsenate was precipitated on the surface of adsorbents proposed by Eq. 6.10 and Fig. 6.7 (Metal oxide formation for iron oxide with As^{5+} path 2) (Wantala et al., 2012).

$$Fe^{2+}/Fe^{3+} + H_2AsO_4^- \rightarrow FeH_2AsO_4 + H_2O \quad (6.9)$$

While, As^{5+} diffused into the oxide surface by solid-phase redox transformation mechanism indicated schematically by Eq. 6.11 (Yan, Vasic, Frenkel, & Koel, 2012)

and Fig. 6.7 (Metal oxide formation for iron oxide with As^{5+} path 3). Arsenate preferred to accumulate at the surface of nZVI-D_2 forming a thin layer of Fe-As intermetallic.

$$FeOOH + H_2AsO_4^- + H^+ \rightarrow FeOAsOOH + 2H_2O \quad (6.10)$$

The last pathway, the existing of diatomite enhanced As^{5+} adsorptions, which is the formation of AsO_2-Si, AsO-Si and As-Al bond proposed by Fig. 6.7 (Metal oxide formation for silica oxide and alumina oxide with As^{5+}path 4). Some As^{5+}ions might be transferred to the surface of diatomite and then As^{5+} was precipitated on adsorbent surface. Thus, Al oxide and Si oxide in diatomite structures plays a significant role in enhanced reactivity and stability of nZVI.

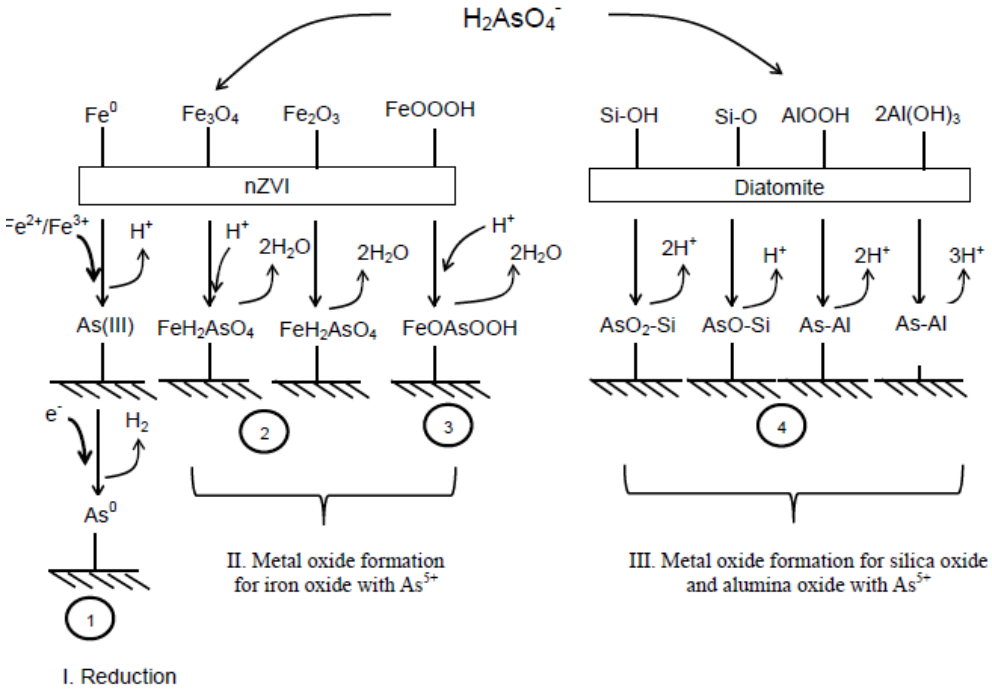

Figure 6.7 Mechanism of arsenate adsorption from aqueous solution by using nZVI-D_2

6.5 Results and discussion of arsenite adsorption process

6.5.1 Optimization of adsorption process of arsenite

CCD can enable to determine regression model of adsorption process, and the quadratic model was used to find out the relationship between the percentage removal (response) as function of adsorbent dose (X_1), pH (X_2) and the initial concentration (X_3) with predicted value shown in the Table 6.3. According to experiment data, the final model equation of estimated regression coefficients for percentage removal of As^{3+} with nZVI-D was explained in terms of coded variables was given in Eq. 6.12.

$$Y = 42.744+12.382X_1-8.595X_2-3.688X_3+1.876X_1^2+1.152X_2^2+0.928X_2^3-8.454X_1X_2-5.724X_2X_3 \quad (6.11)$$

where Y is the predicted response (percentage As^{3+} removal)

The results of the analysis of variance (ANOVA) for quadratic equation are shown in Table 6.7. F-value of 435.02 with p-value less than 0.0001 implied that the response equation demonstrated to be suitable for As^{3+} removal by nZVI-D_2. The equation fits was controlled by coefficient of determination R^2. Based on the results of ANOVA, the equation has high R^2 of 0.9924 and predicted R^2 of 0.9870 which is high correlation between the observed values and the predicted value. This indicated that the regression model gives a good explanation of the relationship between the independent variables and the response. The responses in Table 6.7 illustrated that the linear terms (X_1, X_2, X_3), two quadratic terms (X_1^2, X_2^2, X_3^2) and an interaction terms (X_1X_2, X_2X_3) had a significant effect ($p < 0.05$) on the As^{3+} removal. In contrast, the terms of X_1X_3 had insignificant effect ($p > 0.05$).

Table 6.7 Central composite design designs with experimental value and predicted value of arsenite removal

Run order	Coded levels			% Remove As^{3+}		
	X_1	X_2	X_3	Replicate 1	Replicate 2	Predicted
1	-1	-1	-1	32.70	32.43	32.97
2	1	-1	-1	73.93	71.59	73.54
3	-1	1	-1	43.54	42.80	44.14
4	1	1	-1	52.17	51.62	50.89
5	-1	-1	1	36.13	34.09	35.94
6	1	-1	1	80.53	79.19	78.72
7	-1	1	1	25.96	24.37	24.21
8	1	1	1	33.59	33.91	33.17
9	-1.7	0	0	27.04	28.85	27.11
10	1.7	0	0	67.96	68.37	69.21
11	0	-1.7	0	62.62	59.97	60.68
12	0	1.7	0	30.69	30.57	31.46
13	0	0	-1.7	51.94	53.00	51.69
14	0	0	1.7	38.47	37.85	39.15
15	0	0	0	41.92	42.80	42.74
16	0	0	0	42.53	44.32	42.74
17	0	0	0	42.05	44.78	42.74
18	0	0	0	41.51	44.53	42.74
19	0	0	0	41.73	45.05	42.74
20	0	0	0	40.46	44.50	42.74

Symbols: X_1 = Adsorbent dose, X_2 = pH, X_3 = Initial concentration

Table 6.8 ANOVA for the parameters of response surface quadratic model of arsenite

Source	Sum of squares	df	Mean squares	*F*-value	*p*-value
Regression	8453.65	9	939.29	435.02	0.000
X_1-adsorbent dose	4225.58	1	4225.58	1956.99	0.000
X_2-pH	2036.19	1	2036.19	943.02	0.000
X_3-initial concentration	375.02	1	375.02	173.68	0.000
$X_1 X_2$	1143.62	1	1143.62	529.65	0.000
$X_1 X_3$	4.87	1	4.87	2.26	0.143
$X_2 X_3$	524.30	1	524.30	242.82	0.000
X_1^2	85.07	1	85.07	48.56	0.000
X_2^2	33.31	1	33.31	18.32	0.000
X_3^2	25.68	1	25.68	11.89	0.002
Residual Error	64.78	30	2.16		
Lack of fit	20.82	5	4.16	2.37	0.069
Pure error	43.96	25	1.76		
	8518.42	39			

R^2 = 0.9924, adjusted R^2 = 0.9901 and predicted R^2 = 0.9870

6.5.2 Effect of arsenite adsorption process variables

Contour plots were generated to consider the effect of three factors, such as adsorbent dose, pH and initial concentration on As^{3+} removal. The influences of the three different process variables on the response factors are displayed in the Fig. 6.8.

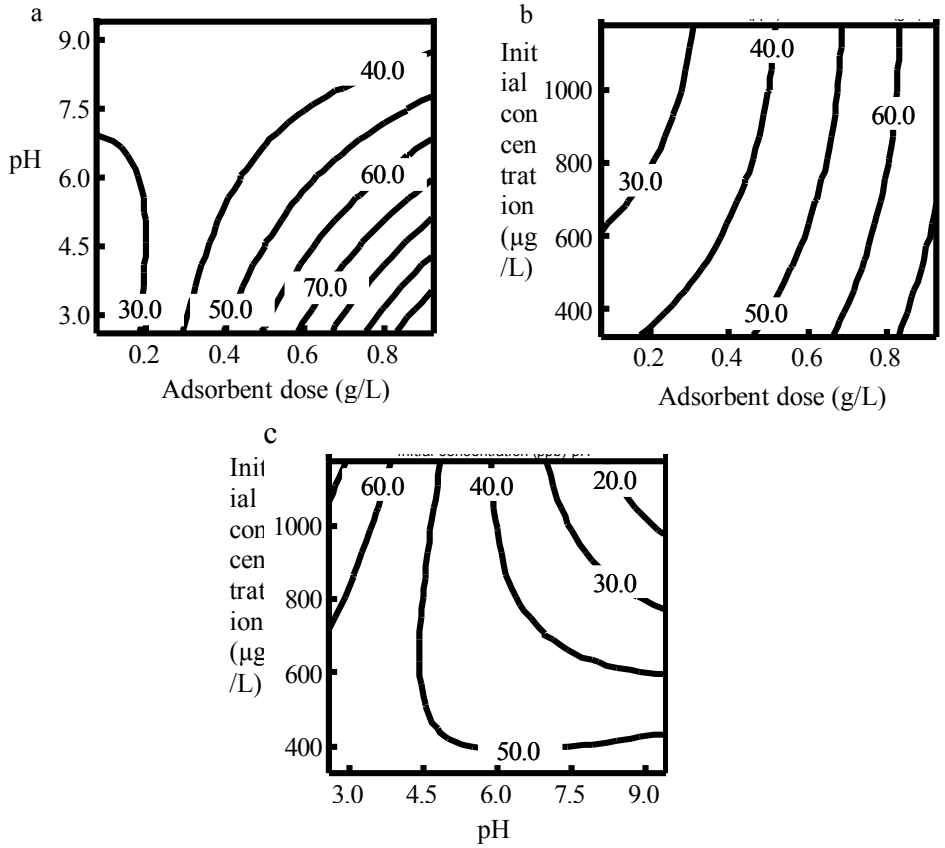

Figure 6.8 Contour plots for combined effect of (a) pH and adsorbent dose (b) initial arsenite concentration and adsorbent dose (c) initial concentration and pH on removal efficiency of arsenite at 1 min

6.5.2.1 Effect of adsorbent dose

Fig. 6.8 show, the effect of adsorbent dose involved the removal efficiency. The percentages removal of As^{3+} increased with adsorbent dosage ranging from 0.075 to 0.925 g/L, It was observed that the removal efficiency increased as the adsorbent dosage was raised. Due to, the total available binding sites of the nZVI-D_2 increased for the specific interactions with the metal ions and adsorbent dosage. It can be explained that the adsorbent dose increased lead to increases in active sites on the surface of adsorbent (Mondal, Majumder, & Mohanty, 2008) and easier infiltrated of a metal ion to the active site (Sarı, Tuzen, Cıtak, & Soylak, 2007). This is, when the dosage of adsorbent is 0.925 g/L, the removal efficiency is almost complete.

6.5.2.2 Effect of pH

The pH of solution is another important factor which affects the removal of heavy metal as it controls ions on the functional groups and protonated or deprotonated on an active site of the adsorbent surface as a result as a result appears a positive or negative surface (Amuda, Giwa, & Bello, 2007). The adsorption occur by the reaction between the active hydrolyzed form of Fe^0, Fe_2O_3 ,$Fe(OH)_3$ and FeOOH on the surface of nZVI-D_2 and As^{3+} that leads to the formation of surface complexes. At the same time, the ions of As^{3+} in the solution depended on the pH which involved the electrostatics interaction between the adsorbent and the adsorbate. For As^{3+}, H_3AsO_3 is the predominant species and presumably the major species being adsorbed at pH 0-6.

The pH effect on the As^{3+} removal efficiency was shown in Fig 6.8. The removal efficiency of As^{3+} decreased with pH ranging from 2.6 to 9.4, this is, pH 2.6 was the best removal. This research contrasts with other research (Chang, Qu, Liu, Liu, & Zhao, 2009; Wu et al., 2014) found that the pH of a weak acid can be treated better than strong acid conditions. The first reason, it can be explanted by the predominant species. When the pH solution is below 6, H_3AsO_3 is the predominant As^{3+} species. The pH of surface charge of nZVI-D_2 was positive ions, this is under acidic conditions (pH < 3) the surface charge becomes more positive. The increase As^{3+} adsorption can be ascribed to the reaction between surface charge of nZVI-D and H_3AsO_3. Whereas, at the pH > 3 of solution more than pH of surface charges as a result the surface of nZVI-D_2 converts negatively charged and electrostatic repulsion between As^{3+} and nZVI-D_2 thus the removal efficiency decreased. The finally season, As^{3+} was reduced with electron of solution in acid condition which become As^0 shown in Eq. 6.13 and the As^0 was adsorbed in inner surface of nZVI-D_2. While the base conditions have the fewer electrons resulting the adsorption of As^{3+} decreased.

$$H_3AsO_3 + O_2 + 2H^+ \rightarrow H_2AsO_4^- + H_2O_2 \quad (6.13)$$

6.5.2.2 Effect of initial concentration

Initial concentration of As^{3+} influences the percentage removal. The effect of initial concentration on the percentage removal is shown in Fig. 6.8. The data indicated that the percentage removal regularly decreased with increasing initial concentration of As^{3+} (325-1,175 µg/L). Due to, the high initial concentration provided less driving force to overcome mass transfer resistances of As^{3+} into film surface of adsorbent (Wu et al., 2014). Another reason, the active site of adsorbent was limited while the initial concentration increased by reason of the removal reaction was intercepted and deceased (Lv, Xu, Jiang, Tang, & Xu, 2012; Mondal et al., 2008).

6.5.3 Optimization and model validation

The optimal conditions is important to study the maximize As^{3+} removal using developed mathematical model. As shown in Fig.6.8, in each plot, one variable was kept constant while the other three were varied within the experimental ranges. The maximum predicted for maximum As^{3+} removal (>100 %) were nZVI-D dose 0.925 g/L, pH 2.6 and initial As^{3+} concentration 1,175 µg/L in the reaction time at 1 min.

6.5.4 Adsorption isotherms of arsenite

Several models have been described experimental data of adsorption isotherms. In this work, Langmuir isotherm, Freundlich isotherm and Dubinin–Radushkevich isotherm models were used to describe the relationship between the adsorbed amount of As^{3+} and its equilibrium concentration in solution which could be shown by the following equation, respectively.

$$\frac{C_e}{q_e} = \frac{C_e}{q_m} + \frac{1}{q_m K_L} \tag{2.3}$$

$$\log q_e = \log k_F + \frac{1}{n}\log C_e \tag{2.5}$$

$$\ln q_e = \ln q_d - \beta\varepsilon^2 \tag{2.6}$$

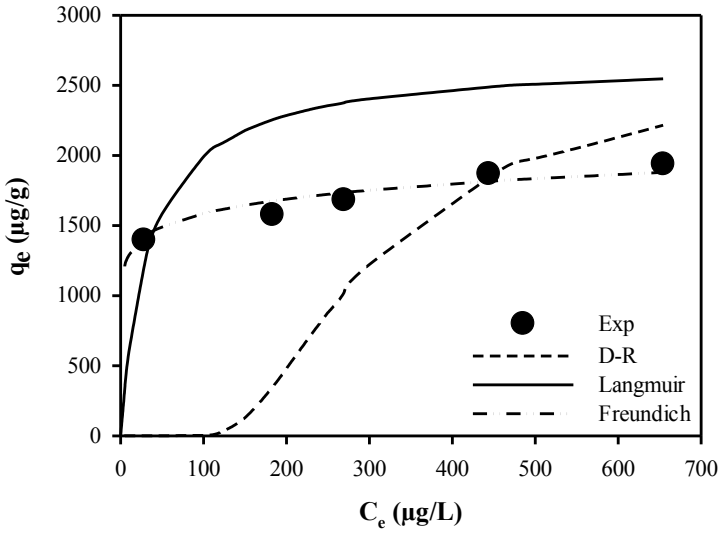

Figure 6.9 Adsorption isotherms of arsenite at initial concentration: 1,000-2,000 µg/g, and pH 6

The Freundlich isotherm, Langmuir isotherm and Dubinin–Radushkevich parameters are display in Table 6.8 and Fig 6.9. The nonlinear As^{3+} adsorption isotherm were given for nZVI-D shown in Fig d. The data indicate that the Langmuir isotherm (R^2 > 0.995) well fit better than Freundlich (R^2 > 0.929) and Dubinin–Radushkevich (R^2 > 0.978) isotherm. It is clear that the adsorption involved the formation of a monolayer of As^{3+} particles coverage on a surface of adsorbent and a surface containing a finite number of adsorption sites of uniform of adsorption (Karagöz, Tay, Ucar, & Erdem, 2008). The values of R_L were in the range of 0-1 indicating that the adsorption process of As^{3+} is favorable for nZVI-D. Additionally values of the Freundlich constant (n) was found 11.037, the adsorption of As^{3+} on nZVI-D_2 was implies stronger interaction between adsorbent and metal ion, the adsorption process is heterogeneous and favorable adsorption (Basu & Ghosh, 2011). The mean free energy (E) of Dubinin–Radushkevich are 6.832 kJ/mol, suggested that As^{3+} adsorption onto nZVI-D is not a physical process (Fan et al., 2008). The maximum adsorption capacity (q_{max}) is 2,682.04 µg/g, which is lower because in this study used initial concentration in the range of 1,000-2,000 µg/L. However, it is higher than or approximate with the results in a previous study (Gupta, Saini, & Jain, 2005; Kundu & Gupta, 2006; Lakshmipathiraj, Narasimhan, Prabhakar, & Bhaskar

Raju, 2006; Su, Huang, Jin, Lu, & Chen, 2011) for instance, Kundu, & Gupta (2006) and Jin Su, et al. (Su et al., 2011) report that the maximum As^{3+} adsorption capacity of iron oxide coated cement is 730 µg/g and surfactant-modified bentonite is 102 µg/g. Furthermore, in the fact of the treatment As^{3+} with nZVI-D_2 can lower than the standard for drinking water (10 µg/g) in 20 min when the initial As^{3+} concentration 1,000 µg/L and adsorbent dosage at 0.75 g/L.

Table 6.9 Langmuir and Freundlich and Dubinin–Radushkevich isotherm parameters for arsenite adsorption on nZVI-D_2 at initial concentration in the range of 1,000-2,000 µg/L, pH 6 and 30 (±0.5) ºC

Langmuir	**constants**	**Freundlich**	**constants**	**Dubinin–Radushkevich**	**constants**
q_{max} (µg/g)	2682.04	n	11.037	q_D (mg/g)	25.96
K_L (L/mg)	0.0287	K_F (mg/g)	10.4464	K_D	0.011
R_L	0.03-0.017	R^2	0.929	E	6.832
R^2	0.995			R^2	0.978

The adsorption capacity of As^{3+} onto nZVI-D_2 as a function of contact time was investigated and records was shown in Fig 6.10. It can be conclude that the adsorption was rapid in first 20 min and the adsorption capacity was equal to 1,228.91 µg/g. In the range of 10 and 20 min, the adsorption capacity was gradually increases from 1,228.91 -1,359.99 µg/g at initial concentration 1,000 µg/g whereas; at 30 min nZVI-D_2 has the adsorption capacity 1,370.70 µg/g of As^{5+} solution. This is a fast uptake was an indicative that the active sites on nZVI-D_2 were readily accessible for As^{3+} adsorption.

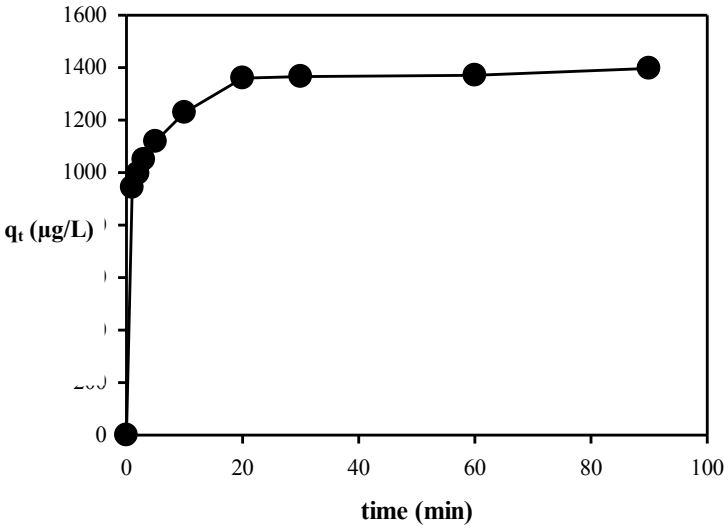

Figure 6.10 Effect of contact time on adsorption of arsenite (initial arsenite concentration: 1,000 µg/L and adsorbent dose: 0.75 g/L)

6.5.4 Kinetic models applied to the adsorption of arsenite

Adsorption kinetics study is important to treatment of aqueous solution. Several kinetics models are used to study the examination of the controlling mechanisms of adsorption process as chemical reaction, diffusion control, and mass transfer (Mahmoodi, Sadeghi, Maleki, Hayati, & Najafi, 2014). Moreover, it describes the solute uptake rate at the solid–solution interface. To demonstrate the adsorption process of arsenic onto nZVI-D_2, a kinetic investigation was used using three kinetic models as pseudo-first-order kinetic model, pseudo-second-order rate and intra-particle diffusion which given by the equation:

$$\log\left(q_e - q_t\right) = \log q_e - \frac{k_1}{2.303} t \tag{2.9}$$

$$\frac{t}{q_t} = \frac{1}{k_2 q_e^2} + \frac{1}{q_e} t \tag{2.10}$$

$$q_t = k_i t^{1/2} \tag{2.12}$$

Table 6.10 Kinetic parameters for the adsorption of As^{3+} onto nZVI-D_2 at the different concentrations

C_o (µg/L)	1,000	1,250	1,500	1,750	2,000
$q_{e,exp}$ (µg/g)	1370.70	1551.12	1662.68	1874.19	1930.76
pseudo-first-order					
$q_{e,cal}$ (µg/g)	681.31	651.70	776.81	1035.11	1053.67
$k_1 \times 10^{-2}$ (L/min)	2.80	2.25	2.65	2.89	2.16
R^2	0.901	0.754	0.807	0.926	0.874
pseudo-second-order					
$q_{e,cal}$ (µg/g)	1378.43	1521.45	1658.85	1865.77	1857.52
$k_2 \times 10^{-3}$ (g/µg·min)	1.05	1.30	0.93	0.61	0.60
R^2	0.995	0.998	0.997	0.995	0.993
intraparticle diffusion					
k_{i1}(mmol·µg·$min^{1/2}$)	133.06	198.15	278.08	302.99	246.70
k_{i2} (mmol·µg·$min^{1/2}$)	6.69	15.86	13.18	11.97	23.41

Tables 6.10 showed the corresponding parameter of the above three kinetic adsorption model which studied various initial concentrations of As^{3+}. It is found that pseudo-second-order kinetic shows well fit experimental kinetic data more than pseudo first-order kinetic and intraparticle diffusion model display in Fig 6.11a-c. The pseudo-second-order kinetic model is based on the ascription that a chemical adsorption involving valence forces through sharing of electrons between nZVI-D_2 and As^{3+} (Hokkanen, Repo, Lou, & Sillanpää, 2015). Thus, the pseudo-second-order kinetic model was likely to describe the overall rate of adsorption process of As^{3+}on nZVI-D. The values of k_2 decrease with increasing of the initial As^{3+}concentration which suggests the downgrade of the diffusion in the solid phase and adsorption rate. It explains that the low initial concentrations of As^{3+} are fast for an adsorption system to reach equilibrium which revealed in Fig 6.12.

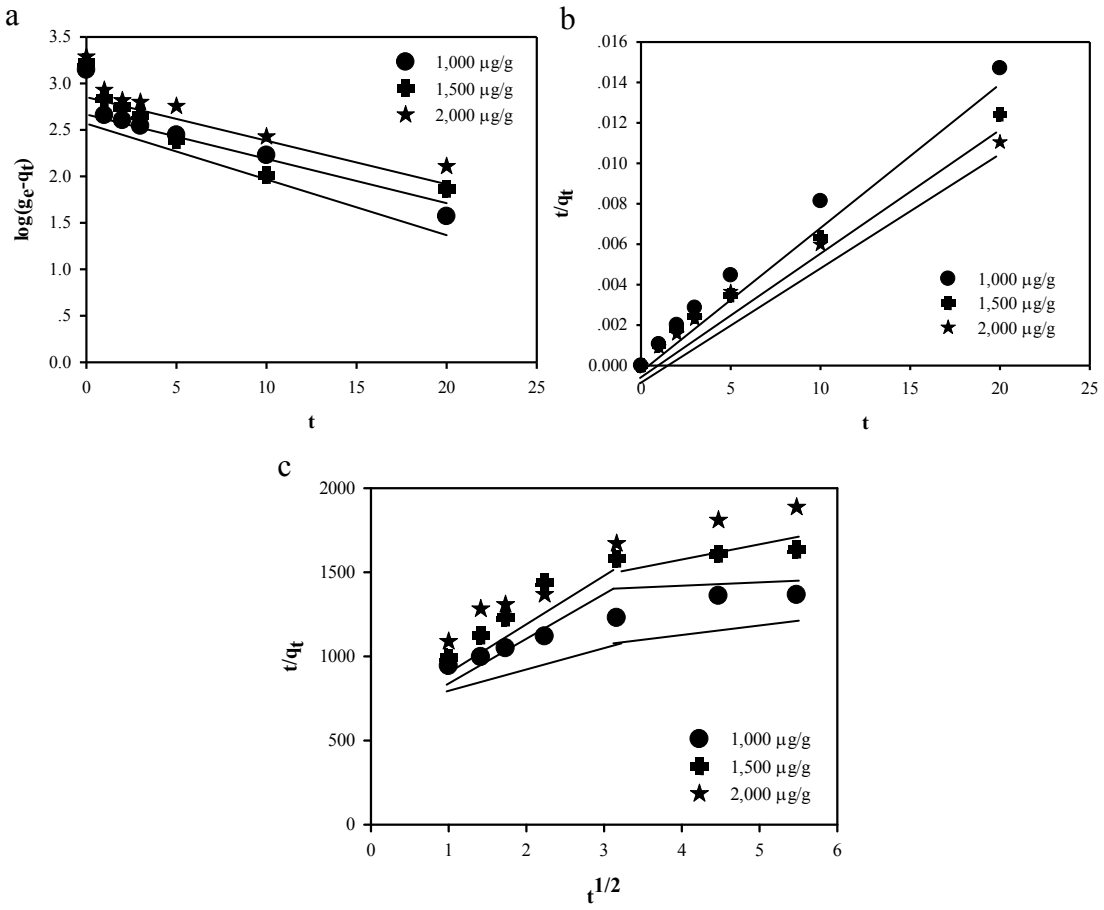

Figure 6.11 (a) Pseudo first-order kinetic (b) Pseudo second-order kinetics (c) intra-particle diffusion kinetic model for arsenite adsorption on nZVI-D_2 at pH 6, adsorbent dose: 0.75 g/L, and temperature: 30 ºC

Nevertheless, both models cannot be explained about external or internal diffusion is the dominant rate limiting step during the adsorption process. The intra-particle diffusion model was able to explain the As^{3+} adsorption process on nZVI-D_2 shown in Fig. 6.11c. It was found that the plots are non-linear. It can divide to three linear, indicating that the process involves more than one kinetic stage in the nZVI-D_2 adsorption. First stage, As^{3+} transfers from the boundary film to surface of nZVI-D_2 (film diffusion). Second stage, As^{3+} transferred from the nZVI-D_2 surface to intraparticle active site or binding site (intra-particle diffusion). Final stage, the adsorption of the As^{3+} diffused on the active or binding sites of nZVI-D_2 until saturation (adsorption). In addition, the data plots do not pass through the origin. This

indicates that the intraparticle diffusion was not rate controlling step. It may be controlled by the film diffusion and intraparticle diffusion (Gupta, & Ghosh, 2009) at the all initial concentration.

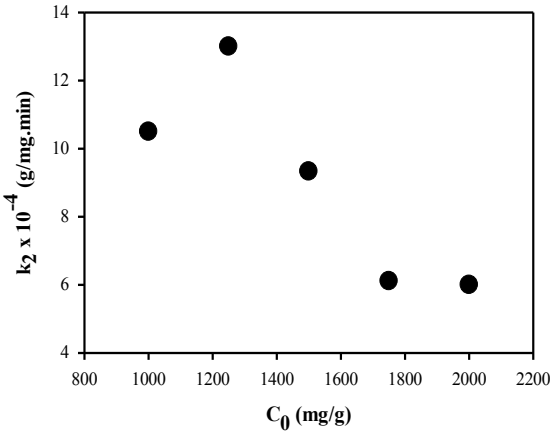

Figure 6.12 Rate constant of pseudo second-order adsorption for arsenite adsorption on nZVI-D_2 at various concentrations (1,000-2,000 µg/g), pH 6, adsorbent dose: 0.75 g/L, and temperature: 30 ºC

6.5.5 Mechanism of arsenite adsorption on nZVI-D

In this study considered the initial solution at pH 6 which the predominate specie of As^{3+} was mainly H_3AsO_3 in solution. The result of XPS found that the oxide outer shell appears FeO, Fe_3O_4, Fe_2O_3 and FeOOH, as determined previously from Fe 2p and O 1s XPS spectra and Fe(0) in the core shell layer. At the same time, it found peak of Si-O, Si-OH, AlOOH and Al(OH) in the nZVI-D_2, this is the structure of diatomite. As^{3+} was adsorbed onto nZVI-D_2 with 5 g/L of adsorbent dose and 100 mg/L of As^{3+} solution (Fig 6.13a), 35.0% of the surface-bound arsenic remained as As^{3+}. Meanwhile, 64.6% of the total arsenic emerged as As^{5+} indicating that As^{3+} oxidation had occurred to significant. However, some researcher found the As^{3+} react reduction to become As^0 (Ramos, Yan, Li, Koel, & Zhang, 2009). Therefore, the reactions of nZVI-D_2 with As^{3+} produced As^0, As^{3+}, and As^{5+} on the nanoparticle surfaces, indicating both reduction and oxidation of As^{3+} occur with nZVI-D_2 removal.

After adsorption, the peak corresponding of Fe^0 was not observed because the Fe^0 was reduce by oxygen and water which became FeO, Fe_3O_4, Fe_2O_3 and

FeOOH display in Fig 6.13b. In addition, the XPS analysis dispaly Si-O, Si-OH, Si-O-M and Al metal which was created after adsorption display in Fig 6.13(c-d). Finally, the result of XPS found the spectrum of As^{3+} had an absorption edge at 44.9 eV while that of As^{5+} was at 45.8 eV.

The removal mechanism can be concluded that As^{3+} was removed by a rapid chemical adsorption, precipitation and important reduction on the nZVI-D_2. A mechanism for As^{3+} removal by nZVI-D_2 is proposed as shown in Fig. 6.14. The mechanism of As^{3+} is similar to As^{5+} whereas, the removal of As^{3+} process raised oxidation process became As^{5+} together shown in Eq. 6.14.

$$H_3AsO_3 + H_2O/O_2 \rightarrow As^{5+} + H_2 \quad (6.14)$$

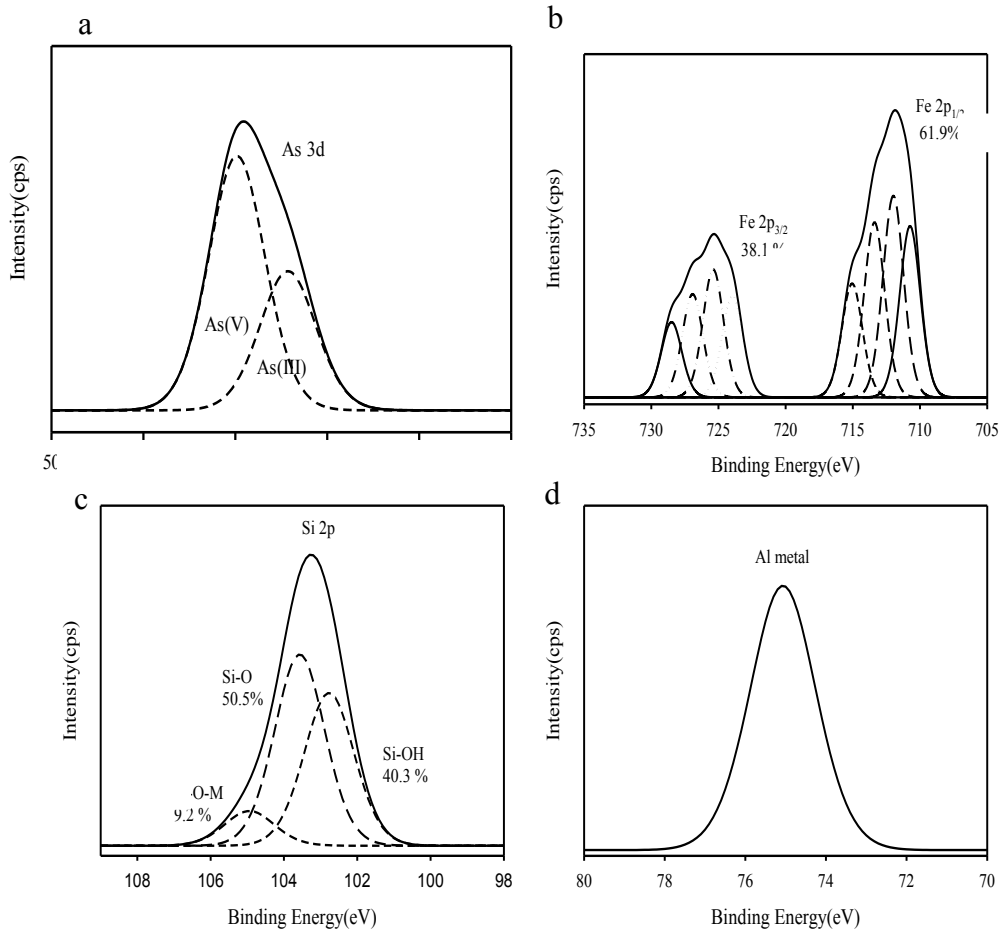

Figure 6.13 XPS spectra of (a) full survey of nZVI-D_2 (b) As 3d (c) Si 2p (d) Al 2p in after adsorption 100 mg/L of arsenite with nZVI-D at 24 hr

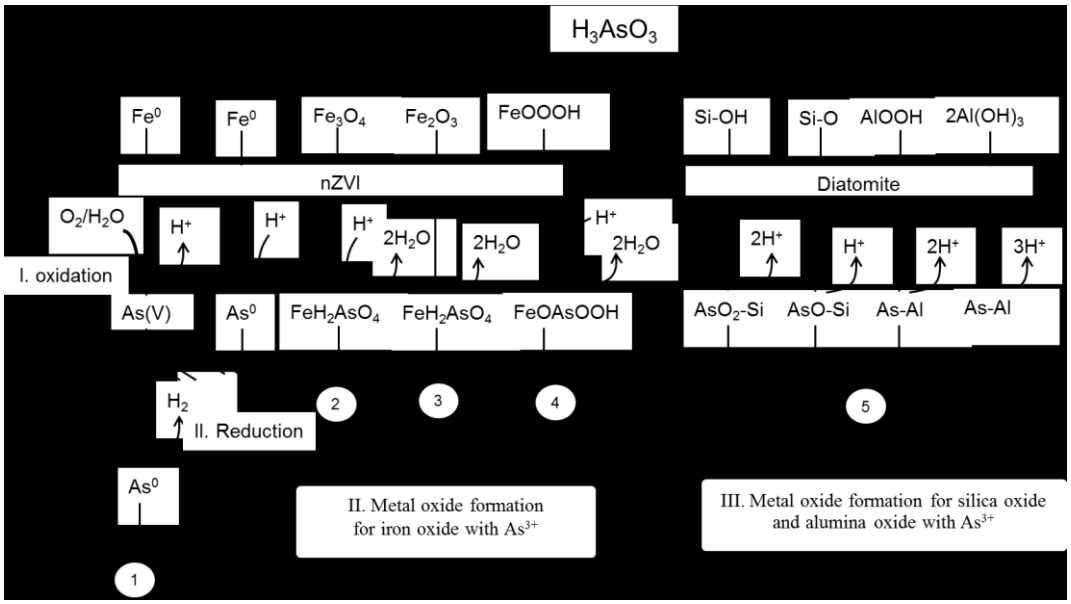

Figure 6.14 Mechanism of adsorption arsenite from aqueous solution by using nZVI-D_2

6.6 Conclusions

In this study, nZVI-D_2 was successfully prepared with a higher capacity and efficiency to remove heavy metals from wastewater. Based on the results, the major conclusions are summarized as follows:

6.6.1 The removal rates of As^{5+} and As^{3+} decrease with an increase of the initial concentrations of heavy metals.

6.6.2 The removal efficiency of As^{5+} and As^{3+} rapidly increased with increase the adsorbent dose.

6.6.3 The percentage of adsorption As^{5+} increases slightly at the pH range of 2.6–6.0 and maximizes at pH 6.0, after pH 6.0, the adsorption of As^{5+} decreases significantly until pH 9.4. While the removal efficiency of As^{3+} decreased with pH ranging from 2.6 to 9.4.

6.6.4 The kinetic adsorption studies showed that the adsorption process well fit followed pseudo-second-order kinetic model. In fact, the intra-particle diffusion model described that mass transfer and intra-particle diffusion were rate-limiting step. At the same time as Langmuir isotherm displayed best fit to the equilibrium adsorption data all of As^{5+} and As^{3+}.

6.6.5 The XPS and XANES results indicated that all of As^{5+} and As^{3+} reduced to As^0 and adsorption, precipitation on the nZVI-D_2. While As^{3+} can oxidation to As^{5+} together.

The results indicated that nZVI-D_2 was effective to remove various heavy metals from wastewater, in terms of efficiency and time, for applications to in situ environmental remediation.

6.7 List of abbreviations

Y	percentages arsenic removal
C_e	equilibrium concentrations solution (mg/L)
C_o	initial solution concentrations (mg/L)
C_t	concentration solution at time (mg/L)
E	mean adsorption energy (kJ/mol)
k_1	rate constant of pseudo-first-order adsorption (min^{-1})
k_2	rate constant of pseudo-second-order adsorption (g/mg·min)
K_D	Dubinin-Radushkevich constant
K_F	Freundlich adsorption constant (L/g)
K_L	Langmuir adsorption constant (L/mg)
k_{i1}	intra-particle diffusion rate constant at slope 1 (mmol/g·$min^{1/2}$)
k_{i2}	intra-particle diffusion rate constant at slope 2 (mmol/g·$min^{1/2}$)
M	mass of adsorbent (g)
n	Freundlich constants
q_e	adsorption capacity at equilibrium (mg/g)
$q_{e.exp}$	adsorption capacity at equilibrium for experimental(mg/g)
$q_{e,cal}$	adsorption capacity at equilibrium for calculated (mg/g)
q_D	adsorption capacity at equilibrium for Dubinin-Radushkevich isotherm (mg/g)
R_L	dimensionless separation factor of Langmuir adsorption
q_{max}	adsorption capacity at equilibrium for Langmuir isotherm (mg/g)
q_t	adsorption capacity at time (mg/g)

R^2	determination coefficients
R^2_{adj}	adjusted determination coefficients
R^2_{pre}	predicted determination coefficients
SD	standard deviation
t	time (min)
V	volume of the solution (L)
Y	response denoted as the predicted $As^{5+/}As^{3+}$ percentage adsorption
X_1	adsorbent dose (g/L)
X_2	pH
X_3	initial concentration (μg/L)

6.8 References

Abdelwahab, O., & Amin, N.K. (2013). Adsorption of phenol from aqueous solutions by Luffa cylindrica fibers: Kinetics, isotherm and thermodynamic studies. **The Egyptian Journal of Aquatic Research, 39**(4), 215–223.

Amuda, O.S., Giwa, A.A., & Bello, I.A. (2007). Removal of heavy metal from industrial wastewater using modified activated coconut shell carbon. **Biochemical Engineering Journal, 36**(2), 174–181.

Arshadi, M., Soleymanzadeh, M., Salvacion, J.W.L., & SalimiVahid, F. (2014). Nanoscale Zero-Valent Iron (NZVI) supported on sineguelas waste for Pb(II) removal from aqueous solution: Kinetics, thermodynamic and mechanism. **Journal of Colloid and Interface Science, 426,** 241–251.

Basu, T., & Ghosh, U.C. (2011). Arsenic(III) removal performances in the absence/presence of groundwater occurring ions of agglomerated Fe(III)–Al(III) mixed oxide nanoparticles. **Journal of Industrial and Engineering Chemistry, 17**(5–6), 834–844.

Bera, A., Kumar, T., Ojha, K., & Mandal, A. (2013). Adsorption of surfactants on sand surface in enhanced oil recovery: Isotherms, kinetics and thermodynamic studies. **Applied Surface Science, 284,** 87–99.

Bhowmick, S., Chakraborty, S., Mondal, P., Van Renterghem, W., Van den Berghe, S., Roman-Ross, G., … Iglesias, M. (2014a). Montmorillonite-supported nanoscale zero-valent iron for removal of arsenic from aqueous solution: Kinetics and mechanism. **Chemical Engineering Journal, 243,** 14–23.

Cao, J., Wu, Y., Jin, Y., Yilihan, P., & Huang, W. (2014). Response surface methodology approach for optimization of the removal of chromium(VI) by NH_2-MCM-41. **Journal of the Taiwan Institute of Chemical Engineers, 45**(3), 860–868.

Chang, F., Qu, J., Liu, H., Liu, R., & Zhao, X. (2009). Fe–Mn binary oxide incorporated into diatomite as an adsorbent for arsenite removal: Preparation and evaluation. **Journal of Colloid and Interface Science, 338**(2), 353–358.

Chen, Z., Zhang, J., Fu, J., Wang, M., Wang, X., Han, R., & Xu, Q. (2014). Adsorption of methylene blue onto poly(cyclotriphosphazene-co-4,4′-sulfonyldiphenol) nanotubes: Kinetics, isotherm and thermodynamics analysis. **Journal of Hazardous Materials, 273,** 263–271.

Dou, X., Li, R., Zhao, B., & Liang, W. (2010). Arsenate removal from water by zero-valent iron/activated carbon galvanic couples. **Journal of Hazardous Materials, 182**(1-3), 108–114.

Elizalde-González, M.P., Mattusch, J., Wennrich, R., & Morgenstern, P. (2001). Uptake of arsenite and arsenate by clinoptilolite-rich tuffs. **Microporous and Mesoporous Materials, 46**(2–3), 277–286.

Fan, T., Liu, Y., Feng, B., Zeng, G., Yang, C., Zhou, M. et al. (2008). Biosorption of cadmium(II), zinc(II) and lead(II) by Penicillium simplicissimum: Isotherms, kinetics and thermodynamics. **Journal of Hazardous Materials, 160**(2-3), 655–661.

Gupta, K., & Ghosh, U.C. (2009). Arsenic removal using hydrous nanostructure iron(III)–titanium(IV) binary mixed oxide from aqueous solution. **Journal of Hazardous Materials, 161**(2–3), 884–892.

Gupta, V.K., Saini, V.K., & Jain, N. (2005). Adsorption of As(III) from aqueous solutions by iron oxide-coated sand. **Journal of Colloid and Interface Science, 288**(1), 55–60.

Gutierrez-Muñiz, O.E., García-Rosales, G., Ordoñez-Regil, E., Olguin, M.T., & Cabral-Prieto, A. (2013). Synthesis, characterization and adsorptive properties of carbon with iron nanoparticles and iron carbide for the removal of As(V) from water. **Journal of Environmental Management, 114,** 1–7.

Hokkanen, S., Repo, E., Lou, S., & Sillanpää, M. (2015). Removal of arsenic(V) by magnetic nanoparticle activated microfibrillated cellulose. **Chemical Engineering Journal, 260,** 886–894.

Kanel, S.R., Grenèche, J.M., & Choi, H. (2006). Arsenic(V) Removal from Groundwater Using Nano Scale Zero-Valent Iron as a Colloidal Reactive Barrier Material. **Environmental Science & Technology, 40**(6), 2045–2050.

Karagöz, S., Tay, T., Ucar, S., & Erdem, M. (2008). Activated carbons from waste biomass by sulfuric acid activation and their use on methylene blue adsorption. **Bioresource Technology, 99**(14), 6214–6222.

Kundu, S., & Gupta, A.K. (2006). Adsorptive removal of As(III) from aqueous solution using iron oxide coated cement (IOCC): Evaluation of kinetic, equilibrium and thermodynamic models. **Separation and Purification Technology, 51**(2), 165–172.

Lakshmipathiraj, P., Narasimhan, B.R.V., Prabhakar, S., & Bhaskar Raju, G. (2006). Adsorption studies of arsenic on Mn-substituted iron oxyhydroxide. **Journal of Colloid and Interface Science, 304**(2), 317–322.

Liu, T., Wang, Z.L., Yan, X., & Zhang, B. (2014). Removal of mercury (II) and chromium (VI) from wastewater using a new and effective composite: Pumice-supported nanoscale zero-valent iron. **Chemical Engineering Journal, 245,** 34–40.

Li, Y., Li, J., & Zhang, Y. (2012). Mechanism insights into enhanced Cr(VI) removal using nanoscale zerovalent iron supported on the pillared bentonite by macroscopic and spectroscopic studies. **Journal of Hazardous Materials, 227-228,** 211–218.

Lv, X., Xu, J., Jiang, G., Tang, J., & Xu, X. (2012). Highly active nanoscale zero-valent iron (nZVI)-Fe_3O_4 nanocomposites for the removal of chromium(VI) from aqueous solutions. **Journal of Colloid and Interface Science, 369**(1), 460–469.

Mahmoodi, N.M., Sadeghi, U., Maleki, A., Hayati, B., & Najafi, F. (2014). Synthesis of cationic polymeric adsorbent and dye removal isotherm, kinetic and thermodynamic. **Journal of Industrial and Engineering Chemistry, 20**(5), 2745–2753.

Mahmood, T., Din, S.U., Naeem, A., Mustafa, S., Waseem, M., & Hamayun, M. (2012). Adsorption of arsenate from aqueous solution on binary mixed oxide of iron and silicon. **Chemical Engineering Journal, 192,** 90–98.

Manning, B.A., Hunt, M.L., Amrhein, C., & Yarmoff, J.A. (2002). Arsenic(III) and Arsenic(V) Reactions with Zerovalent Iron Corrosion Products. **Environmental Science & Technology, 36**(24), 5455–5461.

Ma, W., Lv, T., Song, X., Cheng, Z., Duan, S., Xin, G. et al. (2014). Characteristics of selective fluoride adsorption by biocarbon-Mg/Al layered double hydroxides composites from protein solutions: kinetics and equilibrium isotherms study. **Journal of Hazardous Materials, 268,** 166–176.

Mondal, P., Majumder, C.B., & Mohanty, B. (2008). Effects of adsorbent dose, its particle size and initial arsenic concentration on the removal of arsenic, iron and manganese from simulated ground water by Fe^{3+} impregnated activated carbon. **Journal of Hazardous Materials, 150**(3), 695–702.

Onal, O.T., & Frigi, R.D. (2014). Optimized carbonate micro-particle production by Sporosarcina pasteurii using response surface methodology. **Ecological Engineering, 62,** 168–174.

Örnek, A., Özacar, M., & Şengil, İ.A. (2007). Adsorption of lead onto formaldehyde or sulphuric acid treated acorn waste: Equilibrium and kinetic studies. **Biochemical Engineering Journal, 37**(2), 192–200.

Pojananukij, N., Wantala, K., Neramittagapong, S., & Neramittagapong, A. (2014). Parameter Screening for the Important Factors Influencing the As(V) Adsorption Using a Plackett-Burman Design. **Advanced Materials Research, 931-932,** 178–182.

Ramos, M.A.V., Yan, W., Li, X., Koel, B.E., & Zhang, W. (2009). Simultaneous Oxidation and Reduction of Arsenic by Zero-Valent Iron Nanoparticles: Understanding the Significance of the Core−Shell Structure. **The Journal of Physical Chemistry C, 113**(33), 14591–14594.

Sarı, A., Tuzen, M., Cıtak, D., & Soylak, M. (2007). Adsorption characteristics of Cu(II) and Pb(II) onto expanded perlite from aqueous solution. **Journal of Hazardous Materials, 148**(1–2), 387–394.

Senthil, K.P. (2014). Adsorption of lead(II) ions from simulated wastewater using natural waste: A kinetic, thermodynamic and equilibrium study. **Environmental Progress & Sustainable Energy, 33**(1), 55–64.

Straif, K., Benbrahim-Tallaa, L., Baan, R., Grosse, Y., Secretan, B., El Ghissassi, F. et al, (2009). A review of human carcinogens—Part C: metals, arsenic, dusts, and fibres. **The Lancet Oncology, 10**(5), 453–454.

Su, J., Huang, H.G., Jin, X.Y., Lu, X.Q., & Chen, Z.L. (2011). Synthesis, characterization and kinetic of a surfactant-modified bentonite used to remove As(III) and As(V) from aqueous solution. **Journal of Hazardous Materials, 185**(1), 63–70.

Tatineni, R., Doddapaneni, K.K., Potumarthi, R.C., & Mangamoori, L.N. (2007). Optimization of keratinase production and enzyme activity using response surface methodology with streptomyces sp7. **Applied Biochemistry and Biotechnology, 141**(2-3), 187–201.

Tu, Y.J., You, C.F., Chang, C.K., & Wang, S.L. (2013). XANES evidence of arsenate removal from water with magnetic ferrite. **Journal of Environmental Management, 120,** 114–119.

Wang, C., Luo, H., Zhang, Z., Wu, Y., Zhang, J., & Chen, S. (2014). Removal of As(III) and As(V) from aqueous solutions using nanoscale zero valent iron-reduced graphite oxide modified composites. **Journal of Hazardous Materials, 268,** 124–131.

Wantala, K., Sthiannopkao, S., Srinameb, B., Grisdanurak, N., Kim, K., & Han, S. (2012). Arsenic Adsorption by Fe Loaded on RH-MCM-41 Synthesized from Rice Husk Silica. **Journal of Environmental Engineering, 138**(1), 119–128.

WHO. (2012). **Guidelines for drinking-water quality.** Retrieved November 10, 2012, from http://www.who.int/water_sanitation_health/dwq/guidelines/en/

Wu, Y., Jin, Y., Cao, J., Yilihan, P., Wen, Y., & Zhou, J. (2014). Optimizing adsorption of arsenic(III) by NH_2-MCM-41 using response surface methodology. **Journal of Industrial and Engineering Chemistry, 20**(5), 2792–2800.

Yan, W., Ramos, M.A.V., Koel, B.E., & Zhang, W. (2012). As(III) Sequestration by Iron Nanoparticles: Study of Solid-Phase Redox Transformations with X-ray Photoelectron Spectroscopy. **The Journal of Physical Chemistry C, 116**(9), 5303–5311.

Yan, W., Vasic, R., Frenkel, A.I., & Koel, B.E. (2012). Intraparticle Reduction of Arsenite (As(III)) by Nanoscale Zerovalent Iron (nZVI) Investigated with In Situ X-ray Absorption Spectroscopy. **Environmental Science & Technology, 46**(13), 7018–7026.

Yun, D.M., Cho, H.H., Jang, J.W., & Park, J.W. (2013). Nano zero-valent iron impregnated on titanium dioxide nanotube array film for both oxidation and reduction of methyl orange. **Water Research, 47**(5), 1858–1866.

Zhang, X., Lin, S., Chen, Z., Megharaj, M., & Naidu, R. (2011). Kaolinite-supported nanoscale zero-valent iron for removal of Pb^{2+} from aqueous solution: reactivity, characterization and mechanism. **Water Research, 45**(11), 3481–3488.

Zhang, Y., Li, Y., Li, J., Hu, L., & Zheng, X. (2011). Enhanced removal of nitrate by a novel composite: Nanoscale zero valent iron supported on pillared clay. **Chemical Engineering Journal, 171**(2), 526–531.

Zheng, Y.M., Yu, L., Wu, D., & Paul Chen, J. (2012). Removal of arsenite from aqueous solution by a zirconia nanoparticle. **Chemical Engineering Journal, 188,** 15–22.

Zhuang, Y., Ahn, S., Seyfferth, A.L., Masue-Slowey, Y., Fendorf, S., & Luthy, R.G. (2011). Dehalogenation of polybrominated diphenyl ethers and polychlorinated biphenyl by bimetallic, impregnated, and nanoscale zerovalent iron. **Environmental Science & Technology, 45**(11), 4896–4903.

Zhu, K., Sun, C., Chen, H., Baig, S.A., Sheng, T., & Xu, X. (2013). Enhanced catalytic hydrodechlorination of 2,4-dichlorophenoxyacetic acid by nanoscale zero valent iron with electrochemical technique using a palladium/nickel foam electrode. **Chemical Engineering Journal, 223,** 192–199.